Chapter 7

Thermodynamic Signatures of Macromolecular Complexes – Insights on the Stability and Interactions of Nucleoplasmin, a Nuclear Chaperone

Stefka G. Taneva, Sonia Bañuelos and María A. Urbaneja

Additional information is available at the end of the chapter

http://dx.doi.org/10.5772/54062

1. Introduction

Nucleoplasmin (NP) is a nuclear chaperone that mediates chromatin remodeling processes, such as sperm decondensation at fertilization [1]. In *Xenopus laevis* eggs, where it was first isolated, this highly acidic protein is thought to be in charge of nucleosomal core histones H2A/H2B storage. Upon fertilization, NP decondenses the densely packed sperm chromatin by means of extracting its specific basic proteins and replacing them with H2A/H2B, therefore enabling the assembly of somatic-type nucleosomes. NP is additionally involved in chromatin remodeling during early development, in particular it is required in the replication licensing mechanism, probably to extract linker-type histones from somatic chromatin, and can facilitate pluripotent cell reprogramming. NP (also designated NPM2) belongs to the nucleophosmin/nucleoplasmin family of histone chaperones [2]. Whereas NP roles have been particularly related to fertilization and embryogenesis, nucleophosmin (or NPM1) is ubiquitously and abundantly expressed in adult cells. It is enriched in the nucleolus, and serves multiple functions that affect cell growth and apoptosis, therefore disregulation of NPM1 is linked to several human cancers. Particular mutations of NPM1, that destabilize its structure, and cause its mislocalization to the cytoplasm, trigger acute myeloid leukaemia (AML). Apart from nucleophosmin and NP, the family includes the less known NPM3 and an invertebrate NPM-like.

NP is a homopentameric protein, composed of 200 residues, each subunit being built of two domains, namely core and tail. The core domain, corresponding to the N-terminal 120 residues, adopts an eight-stranded β-barrel structure, and is responsible for oligomerization,

forming a ring with pentameric symmetry of 60 Å (diameter) and 40 Å (height) [3]. This compact core, shared by all NPM family members, confers an extreme stability to NP (see below). Probably, this is mainly due to a conserved network of hydrophobic interactions between the subunits, which, acting as a belt, firmly secures the pentamer. The C-terminal tail domain, instead, is conformationally flexible [4,5], therefore NP is considered "partially disordered" [6]. The tail harbors a segment rich in acidic residues (20 Asp and Glu within residues 120-150) termed "polyGlu", probably involved in histone binding , and a nuclear localization signal (NLS) that directs NP import into the nucleus.

The function of NP is activated through phosphorylation of up to 7 - 10 residues per monomer. NP phosphorylation degree correlates with *Xenopus* egg maturation, so that at the time of fertilization the protein is heavily phosphorylated and displays a maximal chromatin decondensing activity [5,7]. We have identified by mass spectrometry eight phosphorylation sites in natural NP: these phosphoresidues accumulate in flexible regions and loops, along both the core and tail domains, and cluster on a particular pole of the protein, known as distal face [8]. Phosphorylation causes a significant destabilization of the protein and we have made use of calorimetry (differential scanning calorimetry (DSC)) to dissect this effect, and its correlation with NP activation mechanism [9].

To fulfil its chromatin remodeling role, NP has to bind histones, basic proteins needed for packing of DNA. It acts as a reservoir for nucleosomal histones H2A/H2B, and is able to extract sperm specific basic proteins as well as linker-type histones, such as H1 from chromatin. The NP-mediated exchange of these more basic proteins with H2A/H2B results in a looser condensation state of chromatin [1,2]. We have thermodynamically described NP recognition of H2A/H2B and H5, a linker-type histone, by isothermal titration calorimetry (ITC) [10].

NP is the most abundant nuclear protein of *Xenopus* oocytes. Its nuclear import is mediated by the importin α/β heterodimer; in fact, NP is the prototypical substrate of this "classical" pathway, which is in charge of transport of most nuclear proteins [11]. Importin α recognizes a nuclear localization signal (NLS) in its substrates, which consists of a sequence segment with conserved basic residues, and itself associates to importin β [11,12]. The complex formed by importin α/β bound to the NLS cargo, traverses the nuclear envelope through the nuclear pore complexes. The transport relies on a gradient of the small GTPase Ran for directionality. The GTP-bound state of Ran is mostly nuclear and promotes the disassembly of the import complex once it reaches the nucleus, whereas in the cytoplasm, in the presence of Ran-GDP, the import complex formation is favoured [11,12].

Both importin α and β, belong to the karyopherin family of transport receptors, and their structures are constituted by a series of helical repeats, called ARM in the case of importin α and HEAT in importin β, that generate curved, flexible surfaces to bind their ligands. Importin α displays additionally a short N-terminal region for importin β binding (IBB domain) [12]. Most studies on the molecular basis of NLS recognition by nuclear transport receptors are so far limited to isolated domains of the proteins involved (e.g. using peptides corresponding to the NLS of NP and IBB of importin α) [13,14]. We have approached the

thermodynamical characterization of the assembly of the complete complexes made of the full length proteins and have additionally built structural models of those import complexes [15]. NP loaded with histones can additionally incorporate importin α, generating large assemblies that could represent putative NP/histones co-transport complexes [16].

2. Calorimetry: Protein folding/unfolding and binding energetics

Calorimetry (DSC and ITC) is the most precise tool in the study of energetics of thermally-induced conformational transitions of proteins and their assembly with other molecules, small ligands or macromolecules. Extensive reviews have been published on the basic thermodynamic formalism, calorimeters' design and application of DSC [17-20] and ITC [18,20-24]. Moreover, surveys on ITC application are published annually since 2002 [25-28]. Calorimetry on proteins in general will be briefly summarized here and examples for NP will be thoroughly reviewed.

The excess heat capacity of a protein in solution, as a function of temperature, and the heat released or absorbed upon binding interactions are the quantities registered in the DSC and ITC experiments. Both the folding and binding events are described by the Gibbs free energy (ΔG), which determines the stability of the protein and the strength of association of molecules, respectively. The partitioning of ΔG into enthalpic (ΔH) and entropic (TΔS) terms is given by the basic thermodynamic equation:

$$\Delta G = \Delta H - T\Delta S \tag{1}$$

From the experimentally observed calorimetric curve, the DSC thermogram (typically an endothermic peak) and the ITC binding isotherm (exotherm or endotherm), a complete set of thermodynamic parameters of the studied folding/unfolding and binding phenomena is provided.

In DSC the values of the thermodynamic parameters of the folded-unfolded state equilibrium: transition midpoint temperature T_m (the temperature at the maximum of the excess heat capacity curve), the enthalpy of unfolding ΔH, calculated by the integral of the excess heat capacity function:

$$\Delta H = \int_{T_o}^{T_u} c_P dT \tag{2}$$

where T_o and T_u are the temperatures of the onset and completion of the transition, respectively, and c_P (the heat capacity change associated with unfolding) can be determined in a model-independent way [29]. In addition, the width at half-height of the transition $T_{m1/2}$ is a measure of the cooperativity of the transition from folded to unfolded state.

In ITC, the binding affinity K_b ($K_b = e^{-\Delta G/RT}$, R is the gas constant and T is the absolute temperature), the enthalpy change ΔH and the stoichiometry N of the binding interactions are determined by fitting the experimentally obtained binding isotherms assuming a model

that well describes the binding process. While one binding constant describes a simple 1:1 molecular interaction, complex macromolecular recognition processes are described by model-independent macroscopic and model-dependent microscopic association constants, that account for the overall binding behaviour and for the association at each binding site, respectively [30,31]. Model independent analysis of more complex binding data, with two or more binding sites, based on general binding polynomial formalism, developed by Freire et al. [31], allows the type, independent or cooperative, of the binding interactions to be assessed. Methodology and analysis for heterotropic ligand binding cooperativy, i.e. for two or more different ligands binding to one protein has also been elaborated by Velázquez-Campoy et al. [32,33].

ITC is a suitable technique for characterizing allosteric interactions and conformational changes in proteins [32,34-37].

ITC also allows determination of the heat capacity change of binding interactions, Δc_P, from the temperature dependence of the enthalpy change:

$$\Delta c_P = \partial \Delta H / \partial T \tag{3}$$

with the assumption that the apparent heat capacities of the free molecules and the complex are constant over the temperature range under study. The changes in the heat capacity associated with protein-protein binding originate mostly from changes in the hydration heat capacity due to burial of polar and nonpolar groups upon complex formation and the loss of conformational degree of freedom upon binding [38-40]. Hence, Δc_P can be calculated in terms of the change in the accessible surface areas (apolar (ASA_{ap}) and polar (ASA_{pol})) upon the formation of protein-protein complex using the semi-empirical relationship [39,41-42]:

$$\Delta c_P = 0.45 \Delta ASA_{ap} - 0.26 \Delta ASA_{pol} \quad \text{cal } K^{-1} mol^{-1} \tag{4}$$

A good correlation between the experimentally determined and the calculated from structural data Δc_P values has been found in some cases [43-45], however significant difference was reported in other cases [42,46], suggested to be a consequence of changes in the conformational states and significant dynamic restriction of vibrational modes at the surface of the complex, as well as folding transitions coupled to the association event.

The values of Δc_P can also be used to estimate the entropic component due to desolvation of the surfaces of both interacting proteins buried within the binding interface:

$$\Delta S_{solv} = \Delta c_P \ln\left(T / T^*\right) \tag{5}$$

where T* = 385.15 K is the temperature of entropy convergence [47,48] and to further decompose the entropic term, which besides the solvation term contains two more contributions (conformational, ΔS_{conf}, associated with changes in conformational degree of freedom and rotational-translational $\Delta S_{rot\text{-}tr}$, ($\Delta S_{rot\text{-}tr}$ = -7.96 cal $mol^{-1}K^{-1}$ [49] which accounts for changes in rotational/translational degrees of freedom):

$$\Delta S = \Delta S_{solv} + \Delta S_{conf} + \Delta S_{rot-tr} \quad (6)$$

Additional information on protonation/deprotonation effects coupled to the binding interactions can be provided by titration experiments in various buffers of different ionization enthalpy, ΔH_{ion}. The number of protons, n_{H+}, exchanged between the macromolecular complex and the bulk solution, and the binding enthalpy, ΔH_{bind}, can be calculated from the dependence of the calorimetrically observed enthalpy change, ΔH_{obs}, and ΔH_{ion} [42,50,51]:

$$\Delta H_{obs} = \Delta H_{bind} + n_{H+}\Delta H_{ion} \quad (7)$$

To decompose the free energy of binding into electrostatic and non-electrostatic contributions one has to study the ionic strength effect on the binding thermodynamics and analyse the data according to the Debye-Hückel approximation [52].

Valuable information on the hydration or solvent exposure of a polypeptide can be obtained by the absolute heat capacity [29]. A DSC method to accurately determine the absolute heat capacity of a protein from a series of calorimetric thermograms obtained at different protein concentrations has been described in [53]. The slope of a plot of the excess heat capacity versus the protein mass in the calorimetric cell is related to the absolute C_p:

$$m = C_p - \upsilon_p \quad (8)$$

where m is the slope of the linear regression of the plot and υ_p is the partial specific volume of the protein. This information can be related to the integrity of the native state or the presence of residual structure in the denatured state.

The calorimetric transitions in many cases are irreversible and scanning rate dependent, suggesting that the denaturation process is kinetically controlled [54-56]. Appropriate kinetic models were applied to analyse the irreversible unfolding process, after obtaining a set of thermograms at various scanning rates. An irreversible protein denaturation event can be described in some cases by a simplified "two-state irreversible" kinetic model [54,57], assuming that only the native/folded and denatured/unfolded states are significantly populated during the denaturation. Mathematical expressions were derived to calculate the activation energy, E_a, of the denaturation transition [54-58], using diverse experimental information from the calorimetric transition:

i. the values of the rate constant of the transition, k, at a given temperature:

$$k = A \exp\left(-E_a / RT\right) \quad (9)$$

where E_a is the activation energy and A is the frequency factor.

The rate constant of the reaction at a given temperature T is given by:

$$k = \nu\, c_p / \left(Q_t - Q\right) \quad (10)$$

where ν is the scanning rate (K/min), c_P the excess heat capacity at a given temperature, Q is the heat evolved at that temperature and Q_t the total heat of the calorimetric transition.

ii. the dependence of the heat capacity evolved with temperature expressed as:

$$\ln\left[\ln Q_t / \left(Q_t - Q\right)\right] = E_a / R \left(1/T_m - 1/T\right) \quad (11)$$

iii. the heat capacity c_P^m at the transition temperature T_m, where the activation energy can also be calculated by the following eq.:

$$E_a = eRT_m^2 c_P^m / Q_t \quad (12)$$

This "two-state" kinetic model has described the unfolding of bacteriorhodopsin [58], rhodopsin [59], plastocyanin [60], the major light harvesting complex of photosystem II [61], nucleoplasmin (see below, [9]) and some other proteins [62,63]. This model however cannot describe all cases of irreversible protein denaturation [64]. On the other hand, Davoodi et al. [65] have shown that scanning-rate dependence of DSC thermograms is not limited to irreversible processes only.

DSC can also be used to indirectly study ligand binding to proteins and for analysis of very tight binding that can not be analysed by ITC or other spectroscopic methods [66]. In addition, more comprehensive description of the binding energetics can be derived combining the two techniques, ITC and DSC [18].

Recently DSC was also recognized as a novel tool for disease diagnosis and monitoring [67-70]. Calorimetric studies of blood plasma/serum have revealed a typical DSC thermogram for healthy individuals, whereas pronounced changes in thermograms for diseased subjects, including oncopatients, have been reported. Validation of the technique as an efficient tool for disease diagnostics needs further investigations of a large number of diseases.

Besides the classical application of ITC in studies of binding interactions, it has been proven as a powerful technique in diverse fields like drug discovery and lead optimization, nanotechnology, enzyme kinetics, etc. [71,73].

Kinetics of ligand binding to RNA and the subsequent RNA folding have recently been characterized by the so called kinITC [74]. ITC has also permitted documentation of the energy landscape of tertiary interactions along the RNA folding pathway [75]. Thermodynamic parameters, ΔH and Δc_P, of rigid amyloid fibril formation from monomeric β-microglobulin, associated with degenerative disorders have also been determined by ITC [76]. Recently a protocol for novel application of the technique has been elaborated, in which ITC is used as a tracking tool, combined with chromatography, for identification of target protein in biomolecular mixture [77] and it has been suggested to be valuable when the target protein or ligand is unknown. References for the wide spectrum and examples of novel applications of ITC can be found in the surveys published each year in the Journal of Molecular Recognition [25-28].

3. Nucleoplasmin thermal stability. Differential scanning calorimetry

NP is remarkably stable against chemical and physical challenges, including heat; e.g. the T_m of recombinant, non phosphorylated protein is 110.1°C [4,9]. This extreme stability, which is related, as previously mentioned, to the structural scaffolding role of the core domain, is *per se* an attractive issue to be thermodynamically described. We have characterized by DSC and other techniques the stability properties of NP and how they are related to the functionality of the protein. It should be mentioned that the overpressure used in the calorimeter allows to asses melting points above water boiling temperature, by contrast to other spectroscopic techniques.

We have shown that the stability of NP is solely due to the core domain, the T_m of the isolated core (117.6°C) being still higher than that of the full length protein [9]. The slight destabilizing influence of the tail is explained by its strong acidic character, with negatively charged clusters, such as "polyGlu"; electrostatic repulsion is expected to occur between tails and the also negatively charged core domain. This is reflected by the fact that the full length protein is most stable at pH close to its theoretical isoelectric point (pI=5.1), when its stability equals that of the core domain [9].

Analysis of the chemical denaturation of NP by fluorimetric and biochemical techniques has allowed to describe the unfolding mechanism of NP, in terms of a two-state process, where the pentamer dissociation is coupled with unfolding of the monomers, with no evidence of (partially) folded subunits ($N_5 \leftrightarrow 5U$) [78]. Both chemical and thermal unfolding of NP are reversible processes, while denaturation of the isolated core domain is reversible if chemically induced but irreversible upon heating [9,78]. This different behaviour suggests that the charged tail domains favour the solubility of the full length protein after thermal unfolding.

4. Effect of NP activation. Interplay between function and stability

NP activation, mediated by phosphorylation of multiple residues, implies an energetic cost for the protein. We have observed that NP extracted from *Xenopus* oocytes, corresponding to an intermediate phosphorylation state, is significantly destabilized with respect to recombinant, non phosphorylated NP (T_m ~ 94.4°C, ΔH ~ 80 kcal/mol) [4]. Egg NP, which represents the most active protein in the final stage of egg maturation, exhibits a further destabilization (T_m ~ 75°C, ΔH ~ 50 kcal/mol) [9]. This correlation between phosphorylation degree and loss of stability has been also characterized by chemical unfolding experiments [78].

In order to explore the conformational consequences of NP activation, we assessed the impact of phosphorylation in particular sites on the protein stability. Apart from the experimental evidences pointing to CKII and mitosis promoting factor (MPF) as probable kinases that modify NP [7,79], the amount and identity of kinases phosphorylating NP has not been elucidated. On the other hand, NP can be phosphorylated *in vitro* only with very low yield. As an alternative approach to obtain homogeneous preparations of active NP

with a defined modification level, we designed a series of phosphorylation mimicking mutants, in which different Ser and/or Thr residues representing phosphorylatable residues were substituted for Asp [8,9,80]. Most mutation sites correspond to phosphoresidues identified by mass spectrometry analysis of egg NP [9]. However, taking into account that some phosphoresidues might have remained undetected by the proteomic analysis, due to incomplete sequence coverage and/or heterogeneity of the NP natural samples, additional residues were mutated on the basis of prediction software, N-terminal amino acid analysis, sequence comparison within the NP family and structural considerations [8,80].

The mutation sites, which are indicated in Figure 1, can be classified in three groups: 1) mutations in the flexible, N-terminal segment of the protein, not visible in the 3D structure of the core domain (residues 2, 3, 5, 7, 8), 2) mutations of residues located in loop regions of the core domain distal face (15, 66 and 96) and 3) mutations in the tail domain (residues 159, 176, 177, 181 and 183). Apart from the group of three residues within the structured core domain, at least group 1 is expected to face also the distal pole of the protein, which is most probably implicated in histone binding [10,80]. A collection of NP mutants (full length and core domains) were generated, combining the three groups of mutations, as indicated in Figure 1.

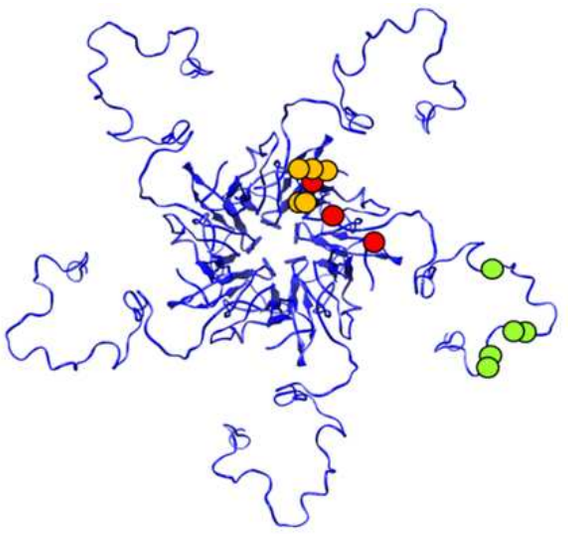

Figure 1. Activation of recombinant NP achieved through phosphomimicking mutations. Their location is highlighted on our model of full length NP based on the crystal structure of the core domain [3] and SAXS data [10]. Orange circles denote substitutions of residues 2, 3, 5, 7, 9 for Asp in the N-terminal segment ("group 1"); red ones correspond to substitutions at 15, 66 and 96 ("group 2"), and green ones to mutations in residues 159, 176, 177, 181, 183 of the tail domain ("group 3"). NP5D carries only mutations in the tail; NP8D harbors groups 1 and 2; NP10D groups 1 and 3; and NP13D comprises all mutations. For the sake of clarity, the positions are shown in only one monomer

By contrast to recombinant, non-phosphorylated NP, which shows negligible ability to decondense chromatin, phosphorylation mimicking mutations render the protein active to varying extents depending on the number and position of mutations**.** The mutants are capable of decondensing *Xenopus* demembranated sperm nuclei and extracting sperm-specific basic proteins, as well as linker-type histones from chromatin. The core domain

isolated from natural, hyperphosphorylated, egg NP is (partly) active in decondensing chromatin, and a recombinant core domain with 8 substitutions (CORE8D, with groups 1 and 2) resembles these functional properties [80]. Nevertheless, full activity can only be attained through accumulation of negative charges (or phosphoresidues) along both the core and tail domains of NP: the mutant NP13D reproduces the functionality of egg NP [8].

Comparison of the thermal unfolding profiles of wild type and mutant core domains reveals that the activating mutations strongly decrease the thermal stability of the protein (Figure 2). Destabilization is probably due to the electrostatic repulsion in the oligomer (already negatively charged at neutral pH), which becomes more intense in the mutants (see inset in Figure 2).

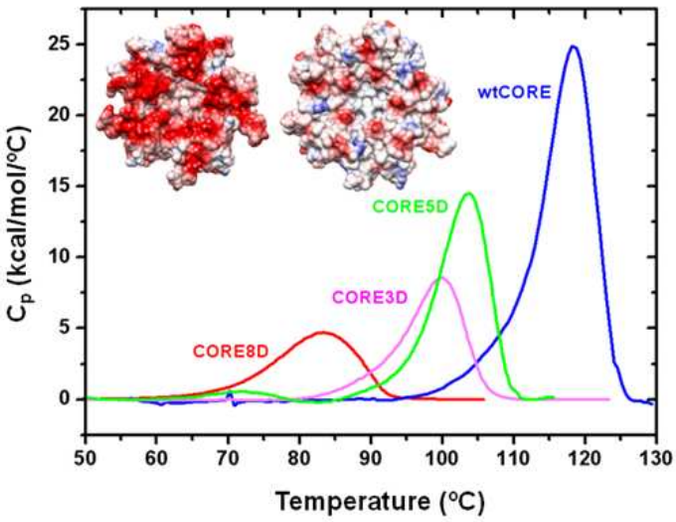

Figure 2. Phosphorylation mimicking mutations decrease the thermal stability of NP core domain. The effect of the mutations on the charge of the protein is also shown, by comparing the surface of the crystal structure of the mutant CORE8D [9] (left) and wild type CORE [3] (right), viewed from the distal face, and colored according to the electrostatic potential

The mutant CORE3D (with group 2 mutations) is less stable, in spite of harbouring fewer substitutions than CORE5D (group 1 mutations), which could be due to the fact that the three residues 15, 66 and 96 locate in structured regions of the protein, whereas the five N-terminal mutations are in a flexible segment that could be re-arranged to alleviate the electrostatic repulsion in NP. The combination of both groups of mutations makes CORE8D the most unstable mutant core, as expected. The strong destabilizing effect (e.g. ΔT_m of 34.5°C in the case of CORE8D) suggests a conformational change in the protein. Phosphorylation does not induce, however, significant changes in the secondary structure of NP [5,9]. Furthermore, we have solved the crystal structure of CORE8D and found that surprisingly enough it is almost identical to that of wild type core domain [9] (see Figure 2).

On the other hand, the activating mutations seem to affect the dynamics of the core domain [9]. The irreversible thermal unfolding of the core can be described as a scanning rate-dependent transition between two states, native and irreversibly denatured. From different mathematical expressions making use of diverse parameters from the calorimetric transition

(eqs. 9-12), the activation energy E_a of the denaturation was calculated and compared for wild type CORE and CORE8D. We obtained a higher E_a value for wtCORE (69.8 ± 2.6 kcal/mol) than for CORE8D (52.1 ± 2.4 kcal/mol), indicating that the mutations destabilize also kinetically the core domain, reducing the energy barrier of the transition to the unfolded state [9]. In addition, to further characterize the conformational change associated with protein activation, the excess heat capacity c_P of wtCORE and CORE8D was measured at various protein concentrations (at 37°C), in order to calculate the absolute heat capacity, C_p, of their native states, which is related to solvent exposure of protein hydrophobic groups (eq. 8, see above). The obtained C_p values were 0.23 and 0.42 cal K^{-1} g^{-1} for wtCORE and CORE8D, respectively, suggesting faster dynamics or faster conformational fluctuations in the mutant [9]. Furthermore, the activation process affects the hydrodynamic properties of the protein (see below).

To understand the contribution of both NP domains to its activation mechanism, we also characterized the function and stability of full length NP, with the three groups of mutations and combinations thereof (Figure 3). Substitutions located in the core domain (NP8D) affect the protein stability to a greater extent than those in the tail domain (NP5D), highlighting again that addition of charges in structurally well defined locations is more deleterious for the stability of the protein than in flexible regions. The most active mutant, NP13D, is also the most unstable (T_m ~ 55.2°C, ΔH ~ 17.9 kcal/mol). Taking into account that at neutral pH aspartic acid has one negative charge, while a phosphoryl group would display an average negative charge of -1.5 [81], 13 Asp would be a reasonable approximation of 7-10 phosphates per monomer in egg NP; however, the fact that this mutant is less stable than egg NP reflects that the conformational properties of phosphorylated NP may not be exactly reproduced [9].

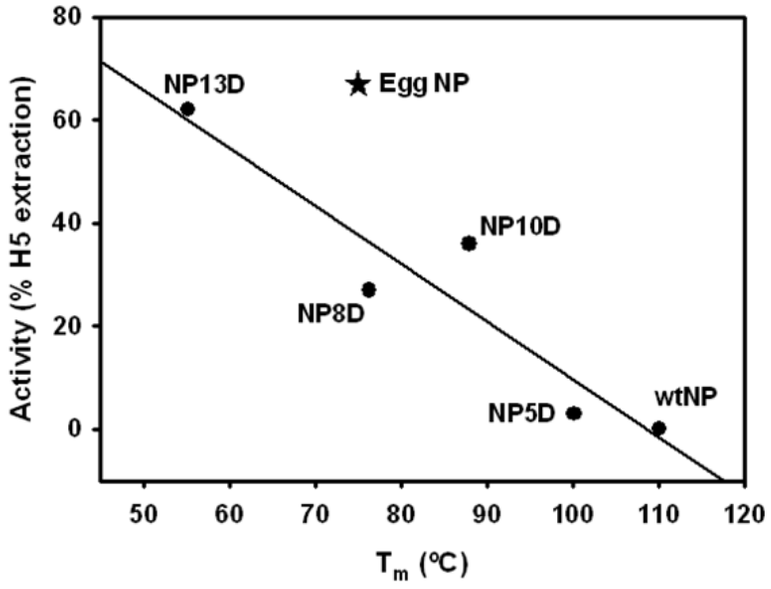

Figure 3. Inverse correlation between NP activity (expressed as percentage of histone H5 extracted from chicken erythrocyte chromatin, in a solubilization assay [8]) and thermal stability (T_m as measured by DSC). Linear regression of the phosphomimicking mutants data is shown

The mutations-induced destabilization of NP is also readily observed by chemical unfolding experiments [9]. Since NP denaturation proceeds through pentamer dissociation intimately coupled to unfolding of the monomers, the activation mechanism, in spite of not affecting conformationally the protein at the level of secondary structure and tertiary structure of the core domain, seems to weaken its quaternary interactions. In support of this notion, we have observed, by size exclusion chromatography and dynamic light scattering, that the activating mutations induce an expansion of the NP pentamer dimensions in solution, both in the core domains (from an average diameter of 64.5 Å to 68.8 Å for CORE8D, as measured by DLS) and the full length mutants (from 93.7 to 99.5 Å in the case of NP13D) [9]. Considering the similarity between the crystal structures of inactive, wild type, and active, mutant core domain, this "swelling" must affect mainly flexible regions of the protein, such as the N-terminal segment, loops of the core domain, and the tail domain.

Therefore, in NP, an inverse correlation exists between activity and stability (Figure 3), the higher the histone chaperone activity performed by NP, the lower its thermal and chemical stability, and larger its dimensions in solution.

In summary, we observed that NP activation mechanism, that depends on the accumulation of negative charge, probably on flexible regions of the distal pole of the protein, implies a destabilizing cost and an expansion of the oligomer in solution. The destabilizing mechanism seems to be the electrostatic repulsion in the pentamer, that weakens the quaternary interactions (tending to "open" apart the structure), which are essential for the stability of this protein. However, the loss of stability does not compromise, under physiological conditions, NP function or folding, which is granted by the extremely stable core domain. Moreover, the activation penalty may explain why this protein, from a mesophilic organism, displays such a remarkable thermal stability: it is necessary to afford the strong destabilization upon activation.

5. Nucleoplasmin chaperoning function studied by isothermal titration calorimetry

The high number of positive charges that histone proteins carry makes them prone to unproductive interactions with nucleic acids and other cellular components. Therefore free histones eventually do not exist within the cellular context and need to be escorted by histone chaperones, which shield their charge, and facilitate their controlled transfer during nucleosome assembly or reorganization. To perform its function, nucleoplasmin has to bind both linker-type and nucleosomal histones. Thermodynamics provided a detailed knowledge of NP-histone complex formation and elicited how NP carries its chaperoning activity [10].

The experimental isotherms of the binding interactions of NP with histones, H5 and H2A/H2B, and the enthalpic and entropic contributions to the Gibbs free energy for the first binding site are summarized in Figure 4.

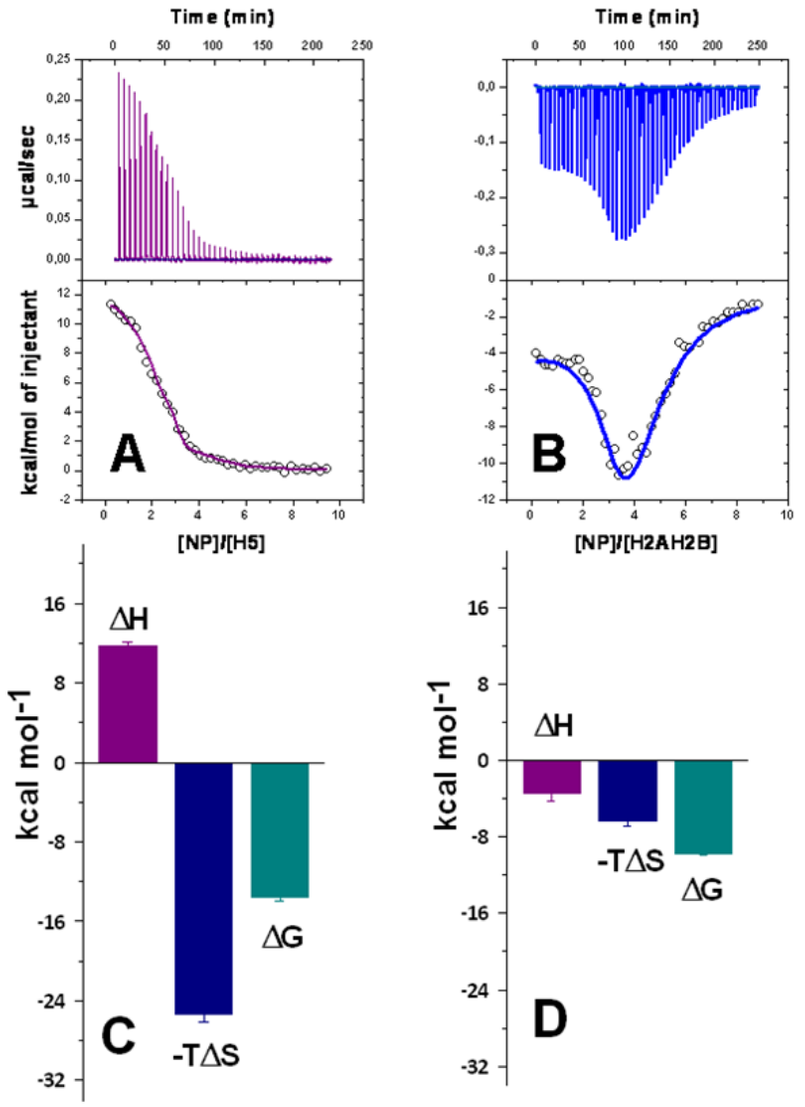

Figure 4. Binding data of NP interactions with the linker, H5, and nucleosomal core, H2A/H2B, histones. (A, B) Baseline-corrected instrumental response of NP titration with successive additions of H5 and H2A/H2B (upper panels); integrated data and the fits of the binding isotherms (solid lines) according to a negative cooperativity model (see text) for H5 and H2A/H2B (lower panels). (C, D) Thermodynamic parameters (ΔG, ΔH, -TΔS) of the assembly of the first histone, H5 and H2A/H2B, molecule with NP

ITC data reveal that NP can accommodate five histone molecules utilizing a negative cooperative binding mechanism with dramatic difference in the binding strength. The binding affinity of histones for the first site is moderate for nucleosomal core (ΔG = −9.8±0.1 kcal/mol, K_b=1.5×10^7 M^{-1}) and extremely high for linker (ΔG = −13.6±0.4 kcal/mol, K_b=10^{10} M^{-1}) histones (Figure 4, C and D), which can provide the basis for its histone exchange capabilities. The binding isotherms of the complex formation of histones with NP were analyzed using a site specific cooperative binding model. The model, developed especially for NP-histone interactions, considers negative cooperative interactions for both adjacently and non-adjacently bound histones and fit the experimental data better than an independent

binding sites model and a general model based on the overall association constants. Eight thermodynamic parameters: four association constants (intrinsic association constant (K) and cooperativity binding parameters: k_1 (associated with the binding of an additional ligand), k_2 (binding of a ligand with contact to one nearest-neighbour) and k_3 (binding of a ligand with contact to two nearest-neighbours)) and four enthalpies were defined in the cooperativity model (details on the model can be found in [10] and in Supplementary Material of [10]).

The binding of histone molecules upon occupancy of the first binding site progresses with an energetic penalty, with exception of H2A/H2B molecules that bind to a non-adjacent site ($k_1 = 1$). Therefore, negative cooperativity was observed for all four additional H5 molecules ($k_1 < 1$), while only for H2A/H2B histone dimers bound to NP adjacently. Since the source of the cooperativity interaction may be an allosteric conformational change in NP induced by histone binding or a direct histone-histone interaction upon binding, or/as well as a combination of both, our results indicate different origin of the negative cooperativity for the binding of H5 and H2A/H2B to NP. Hence the main source of the cooperative binding interaction of H2A/H2B dimers is H2A/H2B-H2A/H2B interaction, whereas a conformational change in the NP pentamer upon binding of the first H5 molecule should provide a less favourable binding interface for the next histone molecules through energetic communication.

Somewhat surprising, considering the strong opposite charge of NP and histones, the binding of both histone types to NP is dominated by a favourable entropic term indicating a strong contribution of the hydrophobic effect to the binding affinity (Figure 4, C and D). The enthalpic term also contributes favourably to the binding energy of H2A/H2B, while unfavourable enthalpy changes counterbalance the entropic contribution to the free energy of H5 binding (Figure 4, C and D).

Furthemore, and contrary to the generally accepted major determinant of tail "polyGlu" tract in histone binding, the thermodynamic analysis as well as the low resolution structural models of NP/histone complexes, constructed by small angle X-ray scattering (SAXS) [10], demonstrate clearly that both NP domains are involved in the interaction with histones.

This was evidenced by comparing the binding energetics of the full-length protein with that of isolated core domain (CORE). Interestingly, NP core domain contributes equally to the intrinsic binding energy of H5 and H2A/H2B (ΔG = -8.2 kcal/mol). The tail domain of NP provides an additional thermodynamic driving force (estimated as the difference between the binding free energies of histones to NP and CORE, $\Delta\Delta G_{NP\text{-}CORE}$) (Figure 4 and Figure 5) for the much stronger binding of H5 ($\Delta\Delta G_{NP\text{-}CORE}^{H5}$ = -5.5 kcal/mol) compared to H2A/H2B ($\Delta\Delta G_{NP\text{-}CORE}^{H2AH2B}$ = -1.6 kcal/mol) suggesting that this domain is particularly essential in the binding to H5 molecules.

To approach an activity/energetics relationship, we analysed the energetics of histone association with NP variants with phosphorylation-mimicking mutations in both the core and tail domains (NP8D, NP13D, CORE, CORE8D).

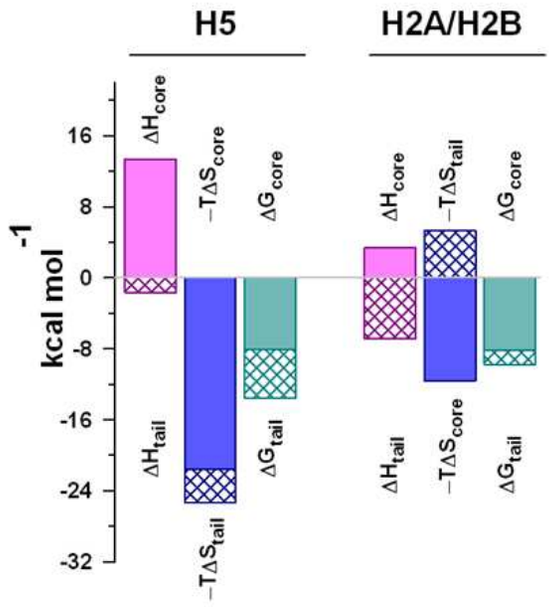

Figure 5. NP core (full bars) and tail (crossed bars) domain contributions to the intrinsic ΔG of their binding to linker and nucleosomal histones

As mentioned above the NP activity is regulated by its phosphorylation state. Insertion of mutations (8 and 13) gradually enhanced the binding affinity and affected to different extent the changes in the Gibbs energy contributors, the entropic and enthalpic terms. This reflects a strong impact of phosphorylation mimicking mutations in both core and tail domains of NP on its recognition by histones (Figure 6). The strongest affinity observed for the NP variant with the highest number of mutations, NP13D, is compatible with the fact that it mimicks the activity of the hyperphosphorylated native protein and can explain the protein activation through post-translational modifications.

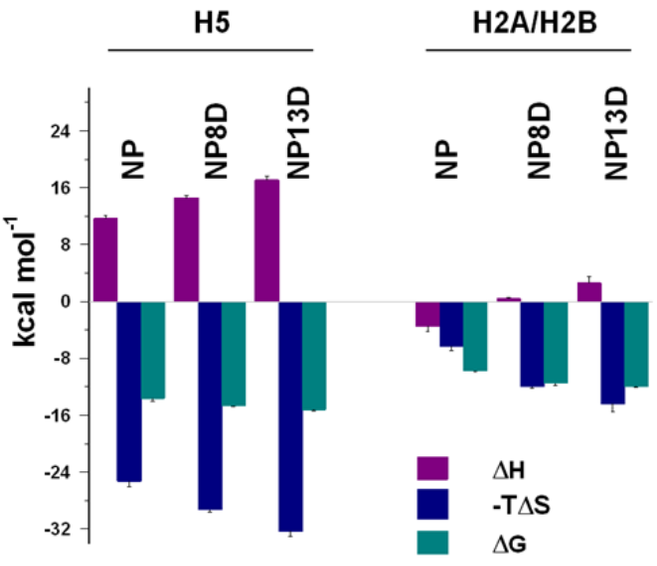

Figure 6. Effect of phosphorylation mimicking mutations on the binding energetics. Bar graphs comparing the intrinsic Gibbs energy, enthalpy and entropy changes, for the intrinsic binding of the two histone types, H5 and H2A/H2B, to NP and the phosphomimicking mutants NP8D and NP13D

Although the hydrophobic interactions are the major source of NP/histone binding free energy (about 80% of the intrinsic free energy for H2A/H2B and about 60% of that for H5), electrostatic and polar interactions between the acidic NP and basic histones also play an important role, either in direct binding or helping in orienting properly the binding partners, given the structural features of NP and histones. In order to get more insight into the nature of binding interactions we studied the ionic strength effect on the binding energetics (Figure 7, left panel). We found that despite the highly charged nature of H5 and NP, the non-electrostatic interactions contribute stronger to the stabilization of NP/histone complexes than the electrostatic ones (Figure 7, right panel). The significantly lower observed free energy of binding ΔG for H2A/H2B compared to H5 originates from lower ΔG_{el} (electrostatic) term (the non-electrostatic term ΔG_{nel} is comparable for H2A/H2B and H5), that should reflect the distinct number of positively charged residues in each histone type. For H2A/H2B and H5 binding to the NP13D mutant ΔG is −9.8±0.1 and -11.9±0.14, and the ΔG_{el} term −2.6 kcal/mol and −5.1 kcal/mol, respectively (Figure 7, right panel).

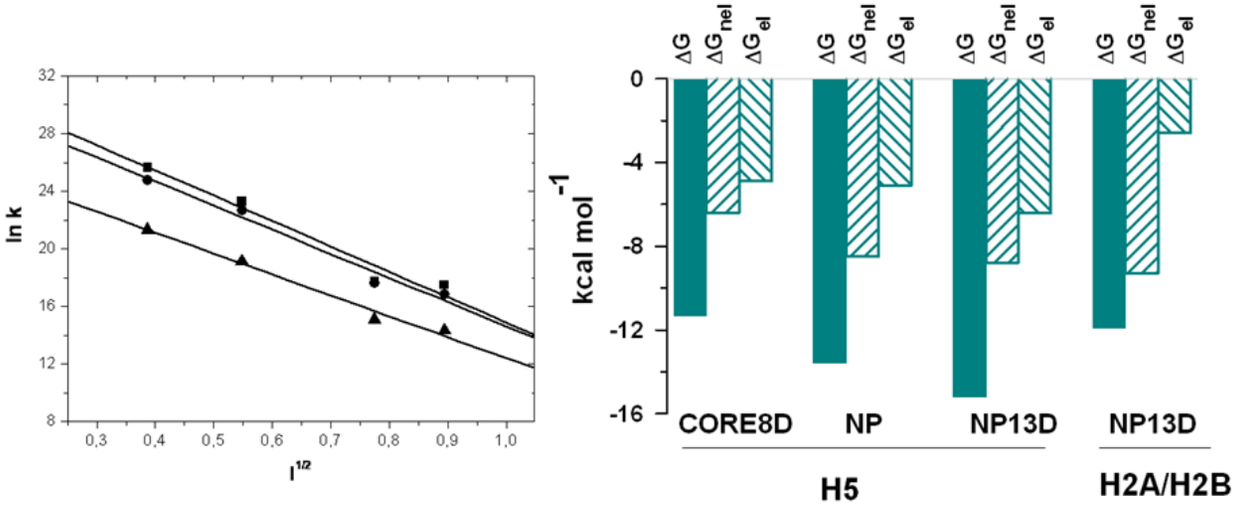

Figure 7. Ionic strength dependence of the association constant of H5 binding to the first (■), non-adjacent (●) and adjacent (▲) binding sites of NP13D variant (left panel). Extrapolation of $\partial \ln(K) / \partial I^{1/2}$ to 1M NaCl yields the non-electrostatic contribution ΔG_{nel} to the binding energy ΔG. Contribution of ΔG_{nel} and the electrostatic contribution, ΔG_{el}, to ΔG for H5 binding to CORE8D, NP and NP13D, and of H2A/H2B to NP13D (right panel)

ITC data also show that the NP flexible tail domain undergoes a histone binding-induced transition to a more structured or ordered state. This follows from the conformational entropy difference between full length proteins and core domains. We estimated from the heat capacity change, that there is a conformational entropy loss of ca. -20 kcal/mol upon H5 binding to the full-length protein as compared to the core domain (and even higher ca. -33 kcal/mol for H5 binding to the mutant proteins, NP8D and CORE8D), that can be attributed to the ordering of the intrinsically disordered nucleoplasmin tails [5] when bound to histones and indicates that NP tails do establish contacts with the histone molecules.

On the other hand, Δc_P (obtained from the temperature dependence of ΔH, presented for the NP13D variant in Figure 8) is smaller for the core domain NP variants compared to the full-

length NP that would indicate a smaller molecular surface area involved in the binding of H5 to the core domain fragments than to full length NP.

Since no high resolution structural data are available for the NP/histone complexes the experimental Δc_P heat capacity changes cannot be compared with the ones estimated from structural data. We therefore roughly estimated the area buried within the binding interface from the SAXS data, in terms of "dummy" atoms of the corresponding "phase" that are in contact with the atoms of another "phase" in MONSA models (for details on SAXS experiments and data analysis see ref.[10]).

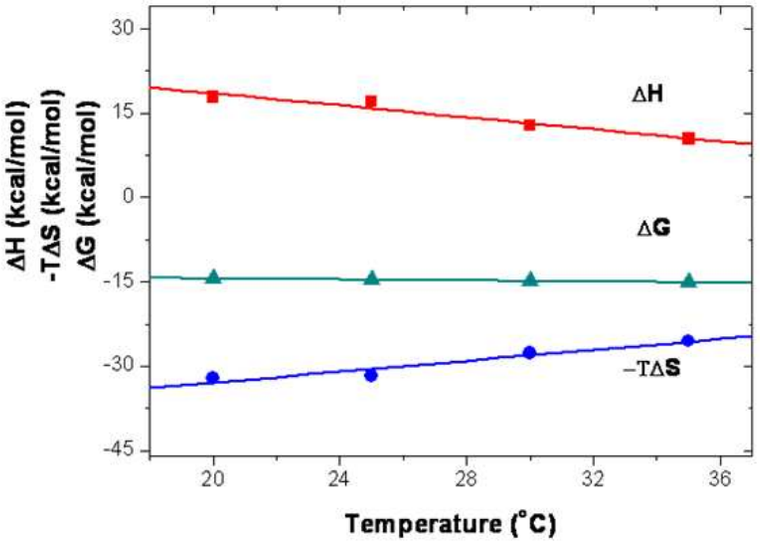

Figure 8. Temperature dependence of the thermodynamic parameters of the binding of the first H5 molecule to NP13D mutant. Intrinsic enthalpy (ΔH, ■), entropy (-TΔS, ●) and free energy (ΔG, ▲) of binding. The heat capacity change Δc_P ($\Delta c_P = (\partial \Delta H/\partial T)$) is determined from linear regression analysis of ΔH data (solid line). The intrinsic free energy of binding is almost independent of temperature reflecting compensation of the enthalpic and entropic terms

The interaction interface area corresponding to NP tail/H5 is approximately double that of NP core/H5, whereas NP tail/H2A/H2B is half of that of NP core/H2A/H2B, which reflects strong difference in the binding of NP tails to both histone types. Although the ratio of the interaction interface areas NP core/NP tails is a rough estimate, it well compares with the ratio estimated from the experimentally determined heat capacity changes, $\Delta c_P^{NPcore}/\Delta c_P^{NPtails}$ ($\Delta c_P^{NPtails} = \Delta c_P^{NP} - \Delta\, c_P^{core}$).

The significant differences between the intrinsic association constants and the cooperative character of NP binding to the nucleosomal and the linker histones defines different "affinity windows" for NP binding from picomolar to nanomolar and from nanomolar to micromolar for H5 and H2A/H2B, respectively. This difference in recognition of nucleosomal and linker histones might provide an efficient mechanism for regulation of the dynamic histone exchange and might allow NP to fulfill its histone chaperone role, simultaneously acting as a reservoir for the core histones and a chromatin decondensing factor. Our data are compatible with the traditional model where NP facilitates nucleosome

assembly by removing the linker histones and depositing H2A/H2B dimers onto DNA [1,2,82].

These data provided new insight into NP/histones assembly and interactions. It should be emphasized that the binding affinity of NP is enhanced upon insertion of phosphorylation-mimicking mutations that explains the protein activation through post-translational modifications. Importantly the data reveal a negative cooperativity-based regulatory mechanism for the linker histone/nucleosomal histone exchange, that in general renders proteins operative in a wider concentration range [83], with significantly populated intermediate liganded states. The employed site-specific cooperativity model, an extension of a previous one that analyses the interaction of another pentameric protein (cholera toxin, with the oligosaccharide portion of its cell surface receptor) considering only nearest-neighbour cooperative interactions [84], has potential application in studies of other macromolecular complexes between proteins sharing structural complexity with NP and their ligands.

6. Recognition of nucleoplasmin and histones by nuclear transport receptors

Nucleoplasmin, that possesses a classical bipartite NLS targeting sequence in each tail domain, is a prototypic substrate of the best characterized route for protein import into the nucleus, which is mediated by importin α/β heterodimer. However, as mentioned in Introduction, most structural and energetic approaches on cargo-import receptor recognition have been achieved merely using peptides carrying the corresponding NLS or IBB sequence [13, 85-91], and to date only two studies (besides ours [10]) deal with assembly of a macromolecular transport complex of full-length proteins [92,93]. On the other hand there has been paid little attention to nuclear import of oligomeric proteins. Therefore understanding the molecular basis of recognition of an oligomeric cargo as nucleoplasmin by its transport receptors, importin α/β heterodimer, would shed light on the arrangement of a large macromolecular nuclear import complex.

We obtained saturated NP/importin α/β complexes proving that all five available NLS binding sites of NP can be occupied by importins. Whereas *in vivo* binding of one α/β heterodimer to any protein should be enough to deliver it to the nucleus, it has been reported that the presence of multiple NLSs in NP [94] enhances its nuclear accumulation, suggesting that the number of NLSs might govern the traffic rate, which would play an advantage for oligomeric nuclear proteins, provided with multiple recognition sites. The binding isotherms of the NP/α/β complex formation (Figure 9A) were well fitted with an independent binding sites model, reflecting that NP makes use of different energetic scheme for assembling with histones and importins, most likely due to the involvement of dissimilar binding surfaces. The binding reaction is enthalpy-driven and counterbalanced by an unfavorable entropy change (Figure 9B) resulting in a relatively high-affinity interaction, $K_b = 18.5 \times 10^6\ M^{-1}$ ($K_d = 57 \pm 15$ nM). The entropic penalty most probably reflects an ordering effect on the otherwise flexible and mobile NLS motifs [5] upon the interaction event. This

loss of conformational flexibility of the NLS segment in the NP tails [5] is estimated to correspond to conformational entropy change ΔS_{conf} = -282 cal mol^{-1} K^{-1} (using eq. 6) that dominates the entropic penalty. This conformational entropy change is unfavorable and greater than the favorable solvation entropy (ΔS_{solv} = 223 cal mol^{-1}K^{-1}, calculated from eq. 5), associated with hydrophobic interactions, thus resulting in an unfavorable entropy contribution to the Gibbs free energy of binding (Figure 9C).

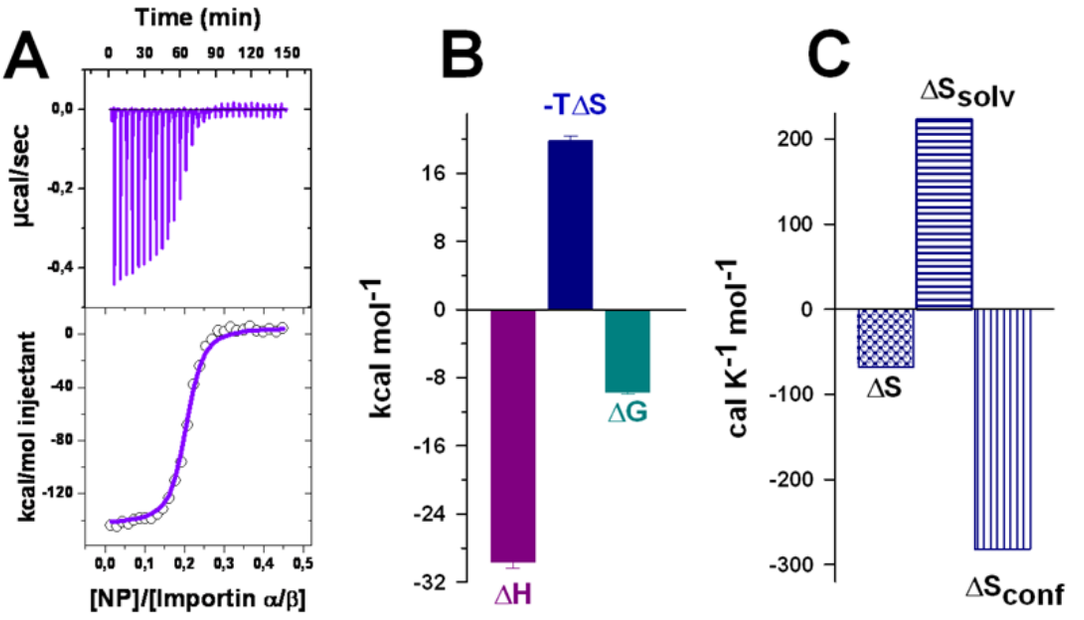

Figure 9. Energetics of NP assembly with the nuclear transport receptor importin α/β. Binding isotherms: the upper panel represents baseline-corrected instrumental response of importin α/β titration with NP; the lower panel shows the integrated data and the fit of the binding isotherm (solid line) by an independent binding site model (A). Enthalpic (ΔH) and entropic (-TΔS) contributions to the free energy (ΔG) of binding (B). Dissection of the binding entropy, ΔS, into solvation, ΔS_{solv}, and conformational, ΔS_{conf}, terms (C)

Similar binding mode and thermodynamic parameters (ΔG = -8.67 ± 0.1 kcal/mol, ΔH = -15 ± 0.3 kcal/mol and stoichiometry 5 per NPM pentamer) characterize the recognition of nucleophosmin (NPM), an abundant nucleolar protein, structurally homologous to nucleoplasmin (as mentioned in the Introduction) and related to oncogenic transformation, by the nuclear transport machinery (unpublished data), which supports an equivalent import mechanism for both chaperones.

Full-length importin α, not assembled with importin β, is also able to bind NP, albeit with a lower apparent affinity (K_d = 513 ± 87 nM) and with a lower enthalpic contribution to the free energy of binding. The loss of apparent affinity comes from the fact that the importin α N-terminal domain, the IBB domain, which contains a similar sequence to the NP-NLS, exerts an autoinhibitory role in the binding process [90,91] because in the absence of importin β, it occupies the NLS binding site and therefore it must be displaced by NP-NLSs. In this regard a truncated importin mutant lacking the IBB domain, ΔIBB-importin α or Δα, shows a similar affinity for NP (K_d = 54 ± 6 nM) as importin α/β [15].

Since protein phosphorylation is one of the mechanisms that up- or down-regulate nuclear transport [95,96] and it had been described that phosphorylated nucleoplasmin presents higher import rate than its unphosphorylated form [79], we studied how phosphorylation of NP affects its interaction with the import receptor. Nevertheless, phosphorylation mimicking mutations in residues close to NLS sequence, as in mutant NP13D, which shows high binding affinity to histones and is active in histone chaperoning, do not modulate the interaction with importin. NP13D mutant displays the same binding strength (ΔG), though different ΔH and –TΔS terms, compared to unphosphorylated protein (Figure 10). No effect has been observed when phosphorylated monopartite NLS from simian virus 40-large T antigen interacts with importin α [97]. Altogether, phosphorylation-mediated regulation of nuclear import must involve interactions other than post-translationally modified NLS with α/β importin.

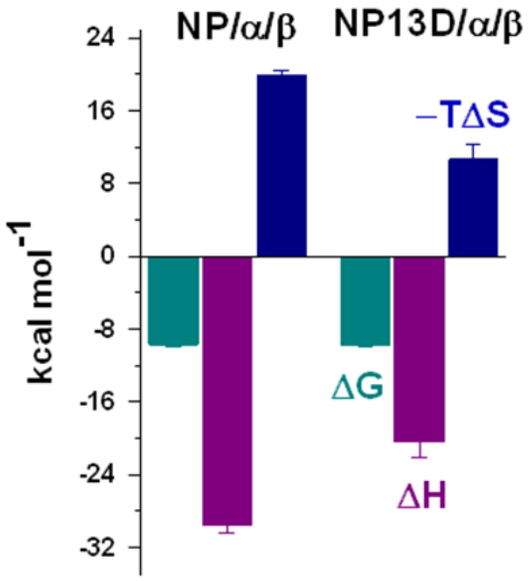

Figure 10. Comparison of the energetics (ΔG, ΔH and -TΔS) of importin α/β binding to NP and NP13D mutant

Importin binds similarly to a peptide corresponding to the NLS sequence when the latter is isolated or in the context of the full-length NP macromolecule, suggesting that no other regions of NP contribute significantly to the binding. The similar large negative Δc_P values, -817 and -796 cal mol^{-1} K^{-1} for NLS and full-length NP respectively, also suggest that the surface area buried within the binding interface is comparable in both cases. It is not surprising that the NLS recognition is not significantly affected by the protein context considering the flexibility displayed by NP tail domains harboring the NLS segments. The same notion applies to the interaction of importin α IBB domain with importin β. The former domain binds likewise to importin β independently of whether it is an isolated peptide or connected to the ARM domain of importin α, as is evidenced by the good correspondence of the heat capacity Δc_P value of -727.4 cal mol^{-1} K^{-1}, predicted from the X-ray structure of importin β bound to the IBB domain of importin α [98], with buried polar

and apolar solvent accessible areas (ΔASA) of 1402.5 and 2426.7 Å^2, respectively (eq. 4), and the experimentally determined Δc_P = -840 cal mol^{-1} K^{-1} value for full length α/β interaction. Moreover, both proteins behave as independent units when they form the heterodimer complex since they display the same thermal stability as the one they exhibit when free in solution, thanks to flexibility of the linker between the IBB and the rest of importin α [15]. These data support the idea that α residues which act as link between both importins exhibit such flexibility that allows each of the importin entities to interact with a wide range of ligands during the nuclear translocation process.

Given the fact that the NP/α/β complexes are formed by multiple proteins that present flexible domains, SAXS technique has provided valuable information about the structure of those assemblies. Multiple models of NP fit equally well the experimental SAXS data reflecting the inherent flexibility of the particle, due to the adaptable linkers between the NP core domain and the NLS (residues 121-154 of NP) [15], which allows the accommodation of five bulky α/β heterodimers per NP pentamer. This 3D in solution structural model, the first one for a complete nuclear transport complex with an oligomeric cargo, is consistent with the notion that the canonical binding elements (NLS and IBB) are the ones determining the molecular basis of the recognition. The multidomain NP/α/β complex remains stable by virtue of two attachment points: recognition of the NLS by importin α and recognition of the IBB domain by importin β, which otherwise allow for conformational flexibility. This modular and articulated architecture might facilitate the passage of such a large particle through the nuclear pore complex.

Due to their highly basic nature histones need nuclear import receptors to be transferred to the nucleus, and most of the pathways described are mainly mediated by karyopherins of β family [99,100]. On the other hand, histones present multiple NLS-like motives and are also recognized by importin α family members for nuclear targeting [101]. Accordingly, we observed that both nucleosomal and linker histones bind to importin β (unpublished data), as previously demonstrated, and to importin Δα [16]. The high affinity exothermic binding interactions (Figure 11) suggest specific recognition events of importin Δα by H5 and H2A/H2B. Regardless of the different stoichiometry, two importin Δα per H5 and one per H2A/H2B, the thermodynamic parameters are quite similar, the apparent binding affinity and the enthalpy are in the order of 9 and 28 nM, and −20 and −17 kcal/mol for H2A/H2B and H5, respectively. Similar binding energetics, though higher stoichiometry (five per NP pentamer), characterizes the assembly of importin Δα with NP (K_d = 54 nM and ΔH = -18.5 kcal/mol, Figure 11). This suggests that similar molecular interactions are involved in the complex formation of importin Δα with the binding motifs of the two histone types and of NP.

Importantly, ITC together with fluorescence anisotropy and centrifugation in sucrose gradients show that NP, histones and importin α can associate and form co-complexes, NP/H5/importin Δα and NP/H2A/H2B/importin Δα of discrete size, that would support a co-transport of histones and NP to the nucleus, mediated by the classical import pathway. Depending on the histone type, linker or core, and the amount of bound histones, different

number of importin Δα molecules can be loaded on NP/histone complexes, in which Δα can bind both to NP-NLS as to histones-NLS-like binding sites, as was demonstrated using a NP mutant with impaired binding to Δα. The binding is an enthalpy driven process and it is characterized by nanomolar affinity [16].

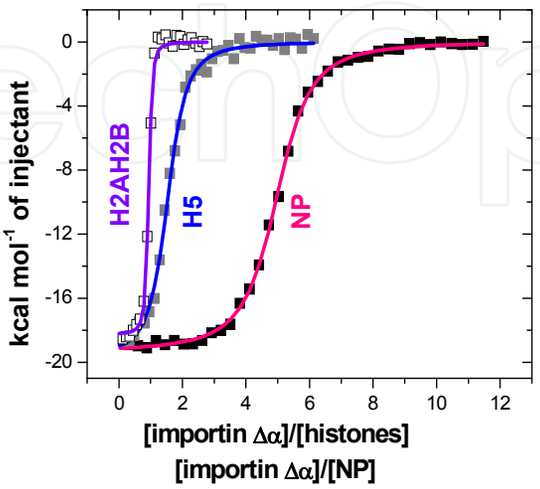

Figure 11. ITC isotherms for the binding interactions of the nucleosomal, H2A/H2B (violet) and linker, H5 (blue) histones, and NP (pink) with importin α ΔIBB (a truncated form lacking the autoinhibitory N-terminal domain)

We have also described the formation of quaternary NP/H5/importin α/β complexes by means of fluorescence and centrifugation, which makes conceivable that α/β heterodimer might "pull" NP/histones complexes into the nucleus, importin α binding either to NP, histones or both. Since importin β binds to both linker and core histones, NP/histones co-transport mediated by importin β, could also be expected. However, this hypothetical route seems unlikely since importin β competes with NP for histones, inducing the release of the latter from NP (unpublished data). Even though no detailed study has been performed, the comparable thermodynamic signature for H5/importin α and H5/importin α/β interaction supports the notion that H5 always binds through importin α in the presence of α/β heterodimer, which would explain the formation of quaternary complexes. Therefore the assembly of NP/histone/importin α/β complexes might have physiological meaning since it supports the existence of a putative and redundant histone import pathway in which positively charged histones would be protected against unspecific interactions by the histone chaperone nucleoplasmin.

7. Conclusion and future prospects

In summary, we have highlighted the importance of calorimetry in the study of nuclear chaperones. Detailed analysis demonstrated that the nuclear chaperone NP can associate with the two histone types and the transport machinery, and that co-complexes of NP, histones, and importins can assemble proving that ITC is suitable to study biological

recognition in complex macromolecular assemblies. Notably, a link between NP phosphorylation state, its stability and the strength with which it assembles with histones is demonstrated.

One key feature of NP assembly with histones is the negative cooperative interactions, that render the protein operative in a wider concentration range and is an effective mechanism of regulation of the activity of macromolecular complexes. We have dissected the thermodynamic cooperativity of NP and its variants, core domain fragments and phosphorylation mimicking mutants, and presented strong evidence of the involvement of both NP domains in binding of histones, the NP tail domain being particularly essential in the assembly with H5 molecules. Only the nuclear localization signal NLS, however, is the recognition site in the multi-component NP/importin α/β complex. The significant differences in the enthalpic and entropic terms of the Gibbs free energy of NP association with histones and importins reflect different energetic strategy for NP chaperoning functions and its recognition for nuclear trafficking.

Both the experimental results and the methodological approach, ITC complemented with SAXS, allow a mechanistic understanding of nucleosome assembly/disassembly and its nuclear trafficking. The NP/histone complexes, which were modeled using five-fold symmetry, have a much more compact shape than the NP/importin α/β complex, reconstructed with multiple models, reflecting inherent flexibility.

Future work should focus towards description of the energetics of NPM export mechanism and the molecular recognition between NPM and nuclear export machinery (exportin), as well as with other proteins and peptides/small molecules. NPM is overexpressed in solid cancers (gastric, colon, ovarian and prostate), while genetic modifications of *NPM1* gene by chromosomal translocation, mutation and deletion are involved in lymphomas and leukemias [102-105]. Mutations of *NPM1* gene result in aberrant cytoplasmic localization of NPM in about 35% of acute myeloid leukemia (AML) patients [102]. The involvement of NPM in human cancer has received an increasing research interest during the last years, but the molecular mechanism of NPM implication in leukaemia and tumorigenesis is not understood yet. Studying the energetics of NPM binding with different (de)stabilizing ligands/drugs would help to regulate its interaction with cellular partners and thereby control its localization and function. This will entail, on one hand knowledge about the NPM nucleo-cytoplasmic shuttling and on the other is expected to provide a strategy for molecular therapeutics.

Author details

Stefka G. Taneva
Unidad de Biofísica (CSIC/UPV-EHU), Departamento de Bioquímica y Biología Molecular, Universidad del País Vasco, Bilbao, Spain,
Institute of Biophysics and Biomedical Engineering, Bulgarian Academy of Sciences, Sofia, Bulgaria

Sonia Bañuelos and María A. Urbaneja
Unidad de Biofísica (CSIC/UPV-EHU), Departamento de Bioquímica y Biología Molecular, Universidad del País Vasco, Bilbao, Spain

8. References

[1] Prado A, Ramos I, Frehlick LJ, Muga A, Ausió J (2004) Nucleoplasmin: a nuclear chaperone. Biochem. Cell Biol. 82, 437-445.

[2] Frehlick LJ, Eirín-López JM, Ausió J (2007) New insights into the nucleophosmin/nucleoplasmin family of nuclear chaperones. Bioessays 29, 49-59.

[3] Dutta S, Akey IV, Dingwall C, Hartman KL, Laue T, Nolte RT, Head JF, Akey CW (2001) The crystal structure of nucleoplasmin-core: implications for histone binding and nucleosome assembly. Mol. Cell 8, 841-853.

[4] Hierro A, Arizmendi JM, Bañuelos S, Prado A, Muga A (2002) Electrostatic interactions at the C-terminal domain of nucleoplasmin modulate its chromatin decondensation activity. Biochemistry 41, 6408-6413.

[5] Hierro A, Arizmendi JM, De las Rivas J, Urbaneja MA, Prado A, Muga A (2001) Structural and functional properties of Escherichia coli-derived nucleoplasmin. A comparative study of recombinant and natural proteins. Eur. J. Biochem. 268, 1739-1748.

[6] Sickmeier M, Hamilton JA, Le Gall T, Vacic V, Cortese MS, Tantos A, Szabo B, Tompa P, Chen J, Uversky VN, Obradovic Z, Dunker AK (2007) DisProt: the Database of Disordered Proteins. Nucleic Ac. Res. 35, D787 – D793.

[7] Cotten M, Sealy L, Chalkley R (1986) Massive phosphorylation distinguishes Xenopus laevis nucleoplasmin isolated from oocytes or unfertilized eggs. Biochemistry 25, 5063–5069.

[8] Bañuelos S, Omaetxebarria MJ, Ramos I, Larsen MR, Arregi I, Jensen OM, Arizmendi JM, Prado A, Muga A (2007) Phosphorylation of both nucleoplasmin domains is required for activation of its chromatin decondensation activity. J. Biol. Chem. 282, 21213-21221.

[9] Taneva SG, Muñoz I, Franco G, Falces J, Arregi I, Muga A, Montoya G, Urbaneja MA, Bañuelos S (2008) Activation of nucleoplasmin, an oligomeric histone chaperone, challenges its stability. Biochemistry 47, 13897-13906.

[10] Taneva SG, Bañuelos S, Arregi I, Falces J, Konarev P, Svergun D, Velázquez-Campoy A, Urbaneja MA (2009). A mechanism for histone chaperoning activity of nucleoplasmin: thermodynamic and structural models. J. Mol. Biol. 393, 448-463.

[11] Görlich D, Kutay U (1999) Transport between the cell nucleus and the cytoplasm. Annu. Rev. Cell Dev. Biol. 15, 607–660.

[12] Stewart M (2007) Molecular mechanism of the nuclear protein import cycle. Nat. Rev. Mol. Cell Biol. 8, 195–208.

[13] Fontes M R, Teh T, Kobe B (2000) Structural basis of recognition of monopartite and bipartite nuclear localization sequences by mammalian importin-α. J. Mol. Biol. 297, 1183–1194.

[14] Catimel B, Teh T, Fontes M R, Jennings IG, Jans DA, Howlett GJ, Nice EC, Kobe B (2001) Biophysical characterization of interactions involving importin-α during nuclear import. J. Biol. Chem. 276, 34189–34198.

[15] Falces J, Arregi I, Konarev P, Urbaneja MA, Taneva SG, Svergun D, Bañuelos S (2010) Recognition of nucleoplasmin by the nuclear transport receptor importin α/β: Insights into a complete transport complex. Biochemistry 49, 9756-9769.

[16] Arregi I, Falces J, Bañuelos S, Urbaneja MA, Taneva SG (2011) The nuclear transport machinery recognizes nucleoplasmin–histone complexes. Biochemistry 50, 7104-7110.

[17] Sánchez-Ruiz JM (1995) Differential scanning calorimetry of proteins. Subcell. Biochem. 24, 133–176.

[18] Jelesarov I, Bosshard HR (1999) Isothermal titration calorimetry and differential scanning calorimetry as complementary tools to investigate the energetics of biomolecular recognition. J. Mol. Recognit.12, 3-18.

[19] Cooper A (1999) Thermodynamics of protein folding and stability. In: Allen G, editor. Protein: A Comprehensive Treatise. JAI Press Inc.Volume 2, pp. 217-270.

[20] Schön A, Velázquez-Capmoy A (2005) Calorimetry In: Jiskoot W, Crommelin DJA, editors. Methods for structural analysis of protein pharmaceuticals. Arlington, VA, AAPS Press. pp. 573-589.

[21] Freire E, Mayorga OL, Straume M (1990) Isothermal titration calorimetry. Anal. Biochem. 179, 131-137.

[22] Laldbury JE, Chowdhry BZ (1996) Sensing the heat: the application of isothermal titration calorimetry to thermodynamic studies of biomolecular interactions. Chem. Biol. 3, 791-801.

[23] Pierce MM, Raman CS, Nall BT (1999) Isothermal titration calorimetry of protein-protein interactions. METHODS 19, 213-221.

[24] Leavitt S, Freire E (2001) Direct measurement of protein binding energetics by isothermal titration calorimetry. Curr. Opin. Struct. Biol. 11, 560-566.

[25] Cliff MJ, Ladbury J (2003) A survey of the year 2002 literature on applications of isothermal titration calorimetry. J. Mol. Recognit. 16, 383-391.

[26] Bjelic S, Jelesarov I (2008) A survey of the year 2007 literature on applications of isothermal titration calorimetry. J. Mol. Recognit. 21, 289-312.

[27] Falconer RJ, Collins BM (2009) Survey of the year 2009: applications of isothermal titration calorimetry. J. Mol. Recognit. 24, 1-16.

[28] Ghai R, Falconer RJ, Collins BM (2011) Applications of isothermal titration calorimetry in pure and applied research - survey of the literature from 2010. J. Mol. Recognit. 25, 32-52.

[29] Freire E (1995) Thermal denaturation methods – study of protein folding. Methods in Enzymol. 259, 144-168.
[30] Brown A (2009) Analysis of cooperativity by isothermal titration calorimetry. Int. J. Mol. Sci. 10, 3457-3477.
[31] Freire E, Schön A, Velázquez-Campoy A (2009) Isothermal titration calorimetry: general formalism using binding polynomials. Methods Enzymol. 455, 127-155.
[32] Velázquez-Campoy A, Goñi G, Peregrina JR, Medina M (2006) Exact analysis of heterotropic interactions in proteins: characterization of cooperative ligand binding by isothermal titration calorimetry. Biophys. J. 91, 1887-1904.
[33] Martinez-Julvez M, Abian O, Vega S, Medina M, Velázquez-Campoy A (2012) Studying the allosteric energy cycle by isothermal titration calorimetry. Methods in Molecular Biology 796, 53-70.
[34] Shiou-Ru T, Charalampos GK (2009) Dynamic activation of an allosteric regulatory protein. Nature 462, 368-374.
[35] Moro F, Taneva SG, Velázquez-Campoy A, Muga A (2007) GrpE N-terminal domain contributes to the interaction with DnaK and modulates the dynamics of the chaperone substrate binding domain. J. Mol. Biol. 374, 1054-1064.
[36] Taneva S, Moro F, Velázquez-Campoy A, Muga A (2010) Energetics of nucleotide-induced DnaK conformational states. Biochemistry 49, 1338–1345.
[37] Seldeen KL, Deegan BJ, Bhat V, Mikles DC, McDonald CB, Farooq A (2011) Energetic coupling along an allosteric communication channel drives the binding of Jun-Fos heterodimeric transcription factor to DNA. FEBS J. 278, 2090-2104.
[38] Sturtevant JM (1977) Heat capacity and entropy changes in processes involving proteins. Proc. Natl. Acad. Sci. U.S.A. 74, 2236-2240.
[39] Spolar RS, Record MT (1992) Coupling of local folding to site-specific binding of proteins to DNA. Science 263, 777-784.
[40] Makhatadze GI, Privalov PL (1995) Energetics of protein structure. Advan. Protein Chem. 47, 307-425.
[41] Murphy KP, Freire E (1992) Thermodynamics of structural stability and cooperative folding behavior in proteins. Adv. Protein Chem. 43, 313-336.
[42] Murphy KP, Xie D, Garcia KC, Amzel LM, Freire E (1993) Structural energetics of peptide recognition: angiotensin II/antibody binding. Proteins: Struct. Funct. Genet. 15, 113-120.
[43] Ladbury JE, Wright JG, Sturtevant JM, Sigler PB (1994) A thermodynamic study of the trp repressor-operator interaction. J. Mol. Biol. 238, 669-681.
[44] Pearce KHJr, Ultsch MH, Kelley RF, de Vos AM, Wells JA (1996) Structural and mutational analysis of affinity-inertcontact residues at the growth hormone-receptor interface. Biochemistry 35, 10300-10307.
[45] Holdgate GA, Tunnicliffe A, Ward WH, Weston SA, Rosenbrock G, Barth PT, Taylor IW, Pauptit RA, Timms D (1997) The entropic penalty of ordered water accounts for

weaker binding of the antibiotic novobiocin to a resistant mutant of DNA gyrase: a thermodynamic and crystallographic study. Biochemistry 36, 9663-9673.

[46] Baker BM, Murphy KP (1996) Evaluation of linked protonation effects in protein binding reactions using isothermal titration calorimetry. Biophys. J. 71, 2049-2055.

[47] Baldwin RL (1986) Temperature dependence of the hydrophobic interaction in protein folding. Proc. Natl. Acad. Sci. U.S.A. 83, 8069–8072.

[48] Murphy KP, Xie D, Thompson KS, Amzel LM, Freire E (1990) Entropy in biological binding processes: estimation of translational entropy loss. Science 247, 559–561.

[49] Luque I, Freire E (1998) Structure-based prediction of binding affinities and molecular design of peptide ligands. Methods Enzymol. 295, 100–127.

[50] Gómez J, Freire E (1995) Thermodynamic mapping of the inhibitor site of the aspartic protease endothiapepsin. J. Mol. Biol. 252, 337-350.

[51] Fukada H, Takahashi K (1998) Enthalpy and heat capacity changes for the proton dissociation of various buffer components in 0.1 M potassium chloride. Proteins: Struct. Func. Genet. 33, 159-166.

[52] Petrucci S (1972) Ionic Interactions 1, 117–177.

[53] Kholodenko V, Freire E (1999) A simple method to measure the absolute heat capacity of proteins. Anal. Biochem. 270, 336–338.

[54] Sánchez-Ruiz JM, López-Lacomba JL, Cortijo M, Mateo PL (1988) Differential scanning calorimetry of the irreversible thermal denaturation of thermolysin. Biochemistry 27, 1648-1672.

[55] Sánchez-Ruiz JM (1992) Theoretical analysis of Lumry-Eyring models in differential scanning calorimetry. Biophys. J. 61, 921-935.

[56] Kurganov BI, Lyubarev AE, Sánchez-Ruiz JM, Shnyrov VL (1997) Analysis of differential scanning calorimetry data for proteins. Criteria of validity of one-step mechanism of irreversible protein denaturation. Biophys. Chem. 69, 125–135.

[57] Freire E, Murphy KP, Sánchez-Ruiz JM, Galisteo ML, Privalov PL (1992) The molecular basis of cooperativity in protein folding. Thermodynamic dissection of interdomain interactions in phosphoglycerate kinase. Biochemistry 31, 250-256.

[58] Galisteo ML, Sánchez-Ruiz JM (1993) Kinetic study into the irreversible thermal denaturing of bacteriorhodopsin. Eur. Biophys. J. 22, 25-30.

[59] Landin JS, Katragadda M, Albert A (2001) Thermal destabilization of rhodopsin and opsin by proteolytic cleavage in bovine rod outer segment disk membranes. Biochemistry 40, 11176-11183.

[60] Milardi D, La Rosa C, Grasso D, Guzzi RC, Sportelli L, Carlo F (1998) Thermodynamic and kinetics of the thermal unfolding of plastocyanin. Eur. Biophys. J. 27, 273-282.

[61] Krumova SB, Todinova SJ, Busheva MC, Taneva SG (2005) Kinetic nature of the thermal destabilization of LHCII Macroaggregates. J. Photochem. Photobiol. B 78, 165-170.

[62] Guzzi R, La Rosa C, Grasso D, Milardi D, Sportelli L (1996) Experimental model for the thermal denaturation of azurin: a kinetic study. Biophys. Chem. 60, 29–38.

[63] Meijberg W, Schuurman-Wolters GK, Boer H, Scheck RM, Robillard GT (1998) The thermal stability and domain interactions of the mannitol permease of *Escherichia coli*. A differential scanning calorimetry study. J. Biol. Chem. 273, 20785-20794.

[64] Lubarev AE, Kurganov BI (2001) Study of irreversible thermal denaturation of proteins by differential scanning calorimetry. Recent Res. Devel. Biophys. Chem. 2,141-165.

[65] Davoodi J, Wakarchuk WW, Surewicz WK, Carey PR (1998) Scan-rate dependence in protein calorimetry: The reversible transitions of *Bacillus circulans* xylanase and a disulfide-bridge mutant. Protein Sci 7, 1538-1544.

[66] Brandts JF, Lin L-N (1990) Study of strong to ultratight protein interactions using differential scanning calorimetry. Biochemistry 29, 6927-6940.

[67] Garbett NC, Miller JJ, Jenson AB, Miller DM, Chaires JB (2007) Interrogation of the plasma proteome with differential scanning calorimetry. Clin. Chem. 53, 2012-2014.

[68] Garbett NC, Miller JJ, Jenson AB, Chaires JB (2008) Calorimetry outside the box: A new window into the plasma proteome. Biophys. J. 94, 1377–1383.

[69] Garbett NC, Mekmaysy C, Helm CV, Jenson AB, Chaires JB (2009) Differential scanning calorimetry of blood plasma for clinical diagnosis and monitoring. Exp. Mol. Pathol. 86, 186-191.

[70] Todinova S, Krumova S, Gartcheva L, Robeerst C, Taneva SG (2011) Microcalorimetry of blood serum proteome – a modified interaction network in the multiple myeloma case. Anal. Chem. 83, 7992-7998.

[71] Ruben AJ, Kiso Y, Freire E (2006) Overcoming roadblocks in lead optimization: A thermodynamic perspective. Chem. Biol. Drug Des. 67, 2–4.

[72] Cai L, Cao A, Lai L (2001) An isothermal titration calorimetric method to determine the kinetic parameters of enzyme catalytic reaction by employing the product inhibition as probe. Anal. Biochem. 299, 19–23.

[73] Chaires JB (2006) A thermodynamic signature for drug–DNA binding mode. Arch. Biochem. Biophys. 453, 26–31.

[74] Burnouf D, Ennifar E, Guedich S, Puffer B, Hoffmann G, Bec G, Disdier F, Baltzinger M, Dumas P (2012) kinITC: A new method for obtaining joint thermodynamic and kinetic data by isothermal titration calorimetry. J. Am. Chem. Soc. 134, 559-565.

[75] Reymond C, Bisaillon M, Perreault J-P (2009) Monitoring of an RNA multistep folding pathway by isothermal titration calorimetry. Biophys. J. 96, 132-140.

[76] Kardos J, Yammamoto K, Hasegawa K, Naiki H, Goto Y (2004) Direct measurement of thermodynamic parameters of amyloid formation by isothermal titration calorimetry. J. Biol. Chem. 279, 55308-55314.

[77] Zhou X, Manjunatha K, Sivaraman J (2011) Application of isothermal titration calorimetry and column chromatography for identification of biomolecular targets. Nature protocols 6,158-165.

[78] Franco G, Bañuelos S, Falces J, Muga A, Urbaneja MA (2008) Thermodynamic characterization of nucleoplasmin unfolding: interplay between function and stability. Biochemistry 47, 7954-7962.

[79] Vancurova S, Paine TM, Lu W, Paine PL (1995) Nucleoplasmin associates with and is phosphorylated by casein kinase II. J. Cell Sci. 108,779–787.

[80] Bañuelos S, Hierro A, Arizmendi JM, Montoya G, Prado A, Muga A (2003) Activation mechanism of the nuclear chaperone nucleoplasmin: role of the core domain. J. Mol. Biol. 334, 585-593.

[81] Tholey A, Lindermann A, Kinzel V, Reed J (1999) Direct effects of phosphorylation on the preferred backbone conformation of peptides: a nuclear magnetic resonance study. Biophys. J. 76, 76–87.

[82] Philpott A, Leno GH (1992) Nucleoplasmin remodels sperm chromatin in *Xenopus* egg extracts. Cell 69, 759-767.

[83] Koshland DEJr (1996) The structural basis of negative cooperativity: receptors and enzymes. Curr. Opin. Struct. Biol. 6, 757-761.

[84] Schön A, Freire E (1989) Thermodynamics of intersubunit interactions in cholera toxin upon binding to the oligosaccharide portion of its cell surface receptor, ganglioside GM1. Biochemistry, 28, 5019–5024.

[85] Conti E, Uy M, Leighton L, Blobel G, Kuriyan J (1998) Crystallographic analysis of the recognition of a nuclear localization signal by the nuclear import factor karyopherin alpha. Cell 94, 193–204.

[86] Conti E, Kuriyan J (200) Crystallographic analysis of the specific yet versatile recognition of distinct nuclear localization signals by karyopherin alpha. Structure 8, 329–338.

[87] Fanara P, Hodel MR, Corbett AH, Hodel AE (2000) Quantitative analysis of nuclear localization signal (NLS)-importin alpha interaction through fluorescence depolarization. Evidence for auto-inhibitory regulation of NLS binding. J. Biol. Chem. 275, 21218–21223.

[88] Fontes MR, Teh T, Jans D, Brinkworth RI, Kobe B (2003) Structural basis for the specificity of bipartite nuclear localization sequence binding by importin-α. J. Biol. Chem. 278, 27981–27987.

[89] Yang SN, Takeda AA, Fontes MR, Harris JM, Jans DA, Kobe B (2010) Probing the specificity of binding to the major nuclear localization sequence-binding site of importin-α using oriented peptide library screening. J. Biol. Chem. 285, 19935–19946.

[90] Kobe B (1999) Autoinhibition by an internal nuclear localization signal revealed by the crystal structure of mammalian importin. R. Nat. Struct. Biol. 6, 388–397.

[91] Harreman MT, Cohen PE, Hodel MR, Truscott GJ, Corbett AH, Hodel AE (2003) Characterization of the auto-inhibitory sequence within the N-terminal domain of importin alpha. J. Biol. Chem. 278, 21361–21369.

[92] Tarendeau F, Boudet J, Guilligay D, Mas PJ, Bougault CM, Boulo S, Baudin F, Ruigrok RW, Daigle N, Ellenberg J, Cusack S, Simorre JP, Hart DJ (2007) Structure and nuclear import function of the C-terminal domain of influenza virus polymerase PB2 subunit. Nat. Struct. Mol. Biol. 14, 229–233.

[93] Dias SM, Wilson KF, Rojas KS, Ambrosio AL, Cerione RA (2009) The molecular basis for the regulation of the cap-binding complex by the importins. Nat. Struct. Mol. Biol. 16, 930–937.

[94] Dingwall C, Sharnick SV, Laskey RA (1982) A polypeptide domain that specifies migration of nucleoplasmin into the nucleus. Cell 30, 449-458.

[95] Jans DA (1995) The regulation of protein transport to the nucleus by phosphorylation. Biochem. J. 311, 705-716.

[96] Hood JK, Silver PA (1999). In or out? Regulating nuclear transport. Curr. Opin. Cell Biol. 11, 241-247.

[97] Fontes MR, Teh T, Toth G, John A, Pavo I, Jans DA, Kobe B (2003) Role of flanking sequences and phosphorylation in the recognition of the simian-virus-40 large T-antigen nuclear localization sequences by importin-α. Biochem. J. 375, 339-349.

[98] Cingolani G, Petosa C, Weis K, Muller CW (1999) Structure of importin-β bound to the IBB domain of importin-alpha. Nature 399, 221–229.

[99] Jäkel S, Albig W, Kutay U, Bischoff FR, Schwamborn K, Doenecke D, Görlich D (1999) The importin beta/importin 7 heterodimer is a functional nuclear import receptor for histone H1. EMBO J. 18, 2411-2423.

[100] Jäkel S, Mingot JM, Schwarzmaier P, Hartmann E, Görlich D (2002) Importins fulfil a dual function as nuclear import receptors and cytoplasmic chaperones for exposed basic domains. EMBO J. 21, 377-386.

[101] Johnson-Saliba M, Siddon NA, Clarkson MJ, Tremethick DJ, Jans DA (2000) Distinct importin recognition properties of histones and chromatin assembly factors. FEBS Lett. 467, 169-174.

[102] Falini B, Mecucci C, Tiacci E, Alcalay M, Rosati R, Pasqualucci L, La Starza R, Diverio D, Colombo E, Santucci A, Bigerna B, Pacini R, Pucciarini A, Liso A, Vignetti M, Fazi P, Meani N, Pettirossi V, Saglio G, Mandelli F, Lo-Coco F, Pelicci PG, Martelli MF (2005) Cytoplasmic nucleophosmin in acute myelogenous leukemia with a normal karyotype.Engl. J. Med. 352, 254-266.

[103] Falini B, Bigerna B, Pucciarini A, Tiacci E, Mecucci C, Morris SW, Bolli N, Rosati R, Hanissian S, Ma Z, Sun Y, Colombo E, Arber DA, Pacini R, La Starza R, Verducci Galletti B, Liso A, Martelli MP, Diverio D, Pelicci PG, Lo Coco F, Martelli MF (2006) Aberrant subcellular expression of nucleophosmin and NPM-MLF1 fusion protein in acute myeloid leukaemia carrying t(3;5): a comparison with NPMc+ AML. Leukemia 20, 368-371.

[104] Falini B, Bolli N, Liso A, Martelli MP, Mannucci R, Pileri S, Nicoletti I (2009) Altered nucleophosmin transport in acute myeloid leukaemia with mutated NPM1: molecular basis and clinical implications. Leukemia 23,11731-1743.

[105] Grisendi S, Mecucci C, Falini B, Pandolfi PP (2006) Nucleophosmin and cancer. Nature Reviews 6, 493-505.

IntechOpen